High-β plasma behaviour in a canted mirror

1973 Nucl. Fusion 13 693

(http://iopscience.iop.org/0029-5515/13/5/007)

HIGH-β PLASMA BEHAVIOUR IN A CANTED MIRROR *

R.A. DANDL, H.O. EASON, A.C. ENGLAND, J.C. SPROTT
Oak Ridge National Laboratory,
Oak Ridge, Tenn.,
United States of America

ABSTRACT. A high-β hot-electron plasma was studied in an asymmetric magnetic mirror device with a variable cant angle. The plasma was produced by microwave heating at a frequency corresponding to cold-electron-cyclotron resonance together with a higher frequency suitable for upper-off-resonance heating. The position of the high-β plasma annulus was studied as a function of cant angle and was found to correspond approximately to the position of a midplane modulus-B contour. High-β effects did modify the spatial location of the losses of energetic electrons into the loss cone but had little effect on the cold-plasma losses. Destabilization was not observed when the line-tying of the plasma centre was reduced with glass end plates. An asymmetry of the cold-plasma loss with respect to the equatorial plane was observed at small cant angles and an electric field model was conjectured to explain this behaviour.

1. INTRODUCTION

As part of a continuing program on electron-cyclotron-heated plasmas at Oak Ridge, a bumpy-torus plasma containment device is under construction. Since the stability of the plasma in this device is based on the formation of high-β relativistic-electron plasma rings in each bump of the torus as observed experimentally in straight mirrors, it seemed wise to study these ring plasmas in non-axisymmetric geometry. The resulting experimental device, called the canted-mirror experiment, could not yield information on high-β toroidal confinement, but very conveniently permitted study of the behaviour of the mirror-confined high-β relativistic-electron annulus.

These high-β electron-cyclotron plasmas, which were first studied at Oak Ridge [1], have the region of maximum plasma energy density located symmetrically around the magnetic axis in an annulus. For some years, these studies were restricted to simple mirror geometry for reasons of diagnostic convenience and simplicity. The canted-mirror experiment incorporated an important parameter variation germane to the design of the ELMO Bumpy Torus (EBT). By having the coils pivoted on axes, the cant angle (the included angle between the planes of the coils) could be varied between 0° and 22°. This allowed a study of a variety of aspect ratios, which is in some ways equivalent to having a variable number of bumps for study.

A previous canted-mirror study was made by Gibson et al. [2] of a low-β plasma composed of cold ions and hot electrons. The present study supplements this original work and incorporates the important aspect of high-β effects.

In section 2 of this paper the experimental arrangement of the canted mirror is described. Section 3 gives some theoretical background on drift surfaces in asymmetric mirrors as well as a description of the effects of error magnetic and electric fields on the plasma behaviour. Section 4 then describes some experiments: observations leading to a description of the shape and size of the high-β annulus; observations of the drift-surface displacement with cant angle; operation with glass end plates to reduce "line-tying"; observation of some peculiar drift-surface effects at small cant angles; and observation of high-β effects on end losses. Finally, section 5 presents some conclusions.

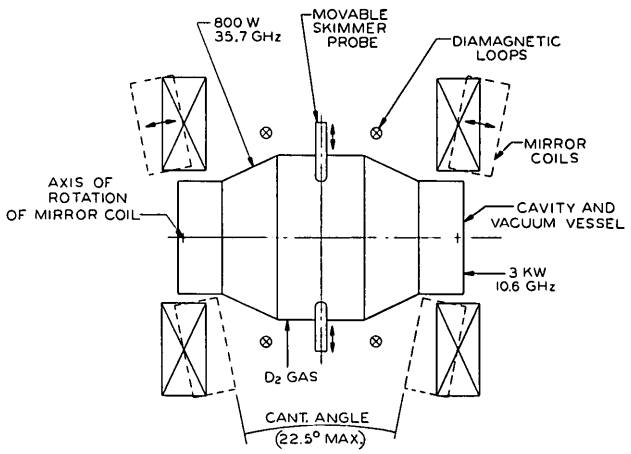

FIG. 1. Schematic diagram of canted-mirror experiment.

2. THE CANTED-MIRROR EXPERIMENT

The canted-mirror experiment is shown schematically in Fig. 1. The mirror coils were canted (or tilted) about parallel axes normal to the magnetic axis by equal and opposite angles. This canting operation could be performed during the actual operation of the machine. The maximum angle between the coils was 22.5° initially. Later the cavity was displaced "inward" (towards the direction of the major axis of an equivalent torus)

* Research sponsored by the US Atomic Energy Commission under contract with the Union Carbide Corporation.

by $\sim \frac{1}{2}$ in., thus permitting only a 15° cant for experiments. The normal mirror ratio of $\sim 2.2:1$ was not significantly changed by this canting operation.

As in the ELMO facility, the device could be fed with both resonant and off-resonant power. A 3-kW cw microwave power source at 10.6 GHz was used for the resonant heating of electrons and an 800-W cw power source at 35.7 GHz was used for the upper-off-resonant heating.

The canted-mirror experiment was equipped with diamagnetic loops, as shown in Fig. 1, which were used to monitor the total stored energy. Also, skimmer probes in the radial ports could be used to intercept the drift surfaces. Extra pumping was later added to one end to improve the vacuum and to reduce the impurity level.

3. CHARACTERISTICS OF THE DRIFT SURFACES IN THE CANTED-MIRROR EXPERIMENT

The confinement of single particles in non-axisymmetric fields can be described conveniently using the second adiabatic invariant, J:

$$J = \int d\ell \sqrt{\frac{2}{m}(\epsilon - \mu B)}$$

where ϵ is the total energy of the particle and μ is the magnetic moment [3]. Except for particles reflected very near the maximum field strength, the surfaces of constant J have circular cross-sections (in the midplane, say) whose centres are shifted towards the major axis by an amount

$$\Delta x = \Delta x_0 \left(1 + \frac{2v_{\parallel}^2(0)}{v_{\perp}^2(0)}\right) \frac{K(k^2)}{2E(k^2) - K(k^2)}$$

where K and E are complete elliptic functions of the argument k^2,

$$k^2 = \frac{v_{\parallel}^2(0)}{(M-1)\, v_{\perp}^2(0)}$$

The shift in the centre of the midplane contours of constant $|\vec{B}|$, Δx_0, is proportional to the cant angle and other geometrical properties of the coils.

M is the mirror ratio along the field line passing through the reference point in the midplane, where $v_{\parallel}$ and $v_{\perp}$ have the values $v_{\parallel}(0)$, $v_{\perp}(0)$. The vanishing of $2E(k_0^2) - K(k_0^2)$ gives rise to the well-known resonance region of velocity-space in which the particle drift surfaces are crescent-shaped and poorly confined in realistic coil configurations.

These effects were first pointed out by Kadomtsev [4], and analysed in greater detail by Morozov and Solovev [5], Gibson, Jordan, Lauer and Woods [6], and recently utilized in an analysis of the drift orbits in the canted-mirror experiment by Guest, Hedrick and Hogan [3]. The validity of the second adiabatic invariant has been supported by numerical computations following single-particle motions [6].

The role of static electric fields has not been explored systematically in the past but has been considered to some extent in the present work because of the observed properties of drift surfaces at small cant angles. Calculations have shown that, in the absence of other effects, small error magnetic fields can have serious consequences in a bumpy torus [7].

Numerical calculations have been made of single-particle orbits in a canted-mirror field. Some direct comparisons of end losses observed in the canted mirror and end losses expected on the basis of these particle-following calculations are shown in section 4.

A computer study of the qualitative effects of error magnetic and electric fields on particle motion was also made. The calculation used the exact three-dimensional relativistic equations of motion and hence did not assume the constancy of either J or μ. Because of computing time limitations, only very energetic particles could be followed. The drift motion in an asymmetric magnetic mirror causes a class of particles to hit walls and be lost, hence some charge separation and a resulting electric field can be expected because of finite-gyrodiameter effects.

The effect of various electric fields on the drift motion of electrons was studied numerically. The electric field was specified in the midplane and calculated elsewhere assuming that the field lines are equipotentials.

Figure 2 shows the effect of a uniform vertical electric field plus an electric field increasing as the square of the distance from a plane below the equatorial plane, plus a small horizontal electric field which is strongest near the axis. These fields satisfy $\nabla \times \vec{E} = 0$ and $\nabla \cdot \vec{E} = -4\pi\rho$. In this case,

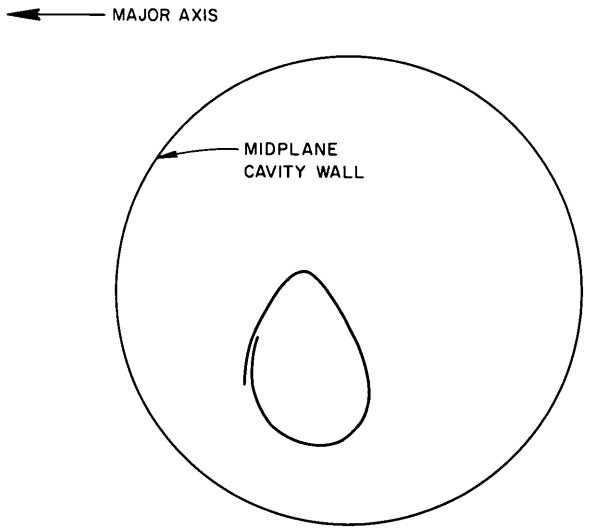

FIG. 2. Drift surface in canted-mirror experiment for a 15° cant and a combination of vertical and horizontal electric fields.

the drift orbit is distorted into a shape qualitatively similar to those found experimentally in the end plate studies in section 4. We have not proven that such fields actually exist in the canted-mirror experiment, only that this is a possible explanation for the observations.

In the case studied the electric field gave electric potential differences across the gyrodiameter corresponding to ~ 1-2% of the electron kinetic energy, E_e, divided by the charge: $\Delta\phi \simeq 10^{-2} \times E_e/e$. Electric fields an order of magnitude larger would cause $\vec{E} \times \vec{B}$-drift out of the machine.

An electric field of the magnitude used in these figures would be difficult to create and maintain in the canted-mirror experiment. However, a small electric field such that $\Delta\phi \sim 10^{-2}\ E_e/e$ across a gyrodiameter for the cold-electron population would only amount to a potential difference of a few volts and hence the cold-electron population could easily be perturbed. The drift surfaces are not a function of the particle's kinetic energy but are a function of the magnetic field shape and the particle's pitch angle. Guest and Harris [8] have suggested small plasma potentials of this magnitude as a stabilizing mechanism in ECH-experiments.

Error magnetic fields similar to those actually present in the canted mirror were also studied numerically. These error fields were due to the uncompensated current leads and gave rise to fields ~ 1% of the midplane magnetic field and normal to it. Fields in the direction of the major radius displaced the drift surface slightly radially (horizontally in the figures). However, for fields normal to the equatorial plane (vertical in the figures), no effect could be observed. These studies showed that the existing error magnetic fields did not seriously perturb the drift surfaces.

We should emphasize that our concern with dc electric fields is based on the indirect experimental evidence presented in sub-section 4. C. 1. We have no direct measurements of electric fields or space potentials. However, the electric field argument is the only known explanation for the experimental observations at this time.

4. EXPERIMENTAL OBSERVATIONS

Some of the initial experiments performed on the canted mirror have been described in a previous publication [9]. These experiments involved probe measurements of the plasma position, bremsstrahlung, and observation of energetic electron end losses. They demonstrated that the canted mirror contained a substantial fraction of the energy in the high-β annulus at cant angles up to 15°. This early observation demonstrated the feasibility of using these high-β annuli in the ELMO Bumpy Torus. In this section, we describe later studies of the properties of high-β plasmas in asymmetric magnetic mirrors.

A. GLASS-END-PLATE EXPERIMENTS

Quartz glass end plates were mounted on both ends of the canted-mirror experiment to study the effect of reduced conductivity of the end walls. This is an important consideration in the bumpy torus where it will not be possible to use line-tying to stabilize the high-β annulus except at its outer edge. Behind the glass end plates was a layer of flowing demineralized water to minimize temperature rise of the glass due to dielectric heating and plasma bombardment. The distance along a field line from the plasma to the outer metallic end outside the glass and water (~ 2 cm) was made as large as possible so as to minimize the capacitive coupling to the conducting outer container wall.

With glass end plates and cooling water, it was necessary to remove the axial pumping and hence the contamination level in the plasma was considerably increased. In addition, the cooling water protecting the glass end plates absorbed some of the microwave power directly. Hence, with the glass end plates, the amount of stored energy in the high-β annulus was slightly more than half as great as with metallic end plates with the same available maximum power as previously. However, no instabilities were found. The neutral pressure required to stabilize the plasma against flute modes was not significantly different with glass end plates. Radial probe scans showed that the annulus did not change its position within the error of the measurement. Pictures of the light from fluorescent material on the metallic outer plate showed the same general position of energetic electron losses as with metallic end plates. However, the detail was not as clear because of the necessity of having the fluorescent material farther from the source of the X-rays.

B. ENERGETIC-ELECTRON END LOSSES ON A FLUORESCENT END PLATE

Energetic-electron end losses from the canted mirror were studied by means of photographs of a fluorescent end plate [9]. It was estimated that electrons with energies $\gtrsim$ 100 keV were required to produce observable light emission. These photographs showed the location of these end losses as the cant angle was increased from zero. The end losses changed from a symmetric ring (due to the annulus) at 0° cant to a bright region on the "inside" of the end plate at 15° cant. One of these photographs was compared to the unperturbed drift surface trajectories discussed in section 3. Figure 3 shows the 15°-cant-angle fluorescent plate photograph. Superimposed on this photograph are some numerically calculated trajectories of 1-MeV electrons which have pitch angles causing them to execute large excursions into the mirror throats. The three trajectories shown are for electrons that have pitch angles within one degree of the maximum allowed for containment at some point on the trajectory. The trajectories shown are the projections of the intersection of the drift surface at a plane far into the mirror throat onto the end plate along the calculated magnetic field lines.

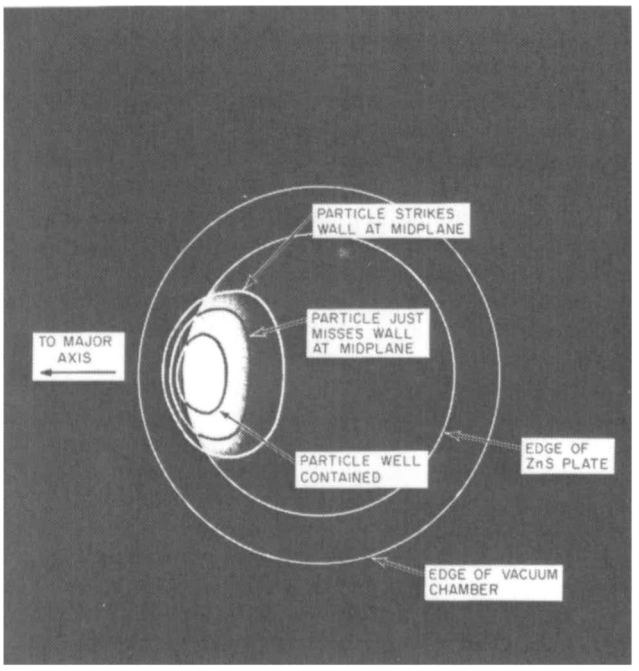

FIG. 3. Computed drift surface compared to energetic electron end losses in the canted mirror, $\theta_c = 15°$

The particle whose drift surface strikes the wall at the midplane should not be observed on the end plate and no evidence is seen for it. The photograph shows a demarcation in the fluorescent intensity about at the position expected for particles just missing the wall at the midplane. Particles well inside the midplane wall would produce the bright central portion of the illumination on the end plate.

The particles must scatter by a small angle from their contained drift surfaces to arrive at the end plate. The assumption is made that the trajectory can be projected along the field lines because the particle will only have to scatter ~ 0.01 radian to escape from the mirror for the cases illustrated in this figure.

This study indicated that the agreement between drift-surface calculations and experiment was excellent. Because of the difficulty of interpreting intensities on photographic film, no high-β studies were possible with the fluorescent end plate.

C. TEMPERATURE PATTERNS ON CAVITY WALLS AND ENDS

A thin stainless-steel end plate was used in observing the temperature patterns resulting from plasma losses to the ends (i.e. losses out of the mirror throat) of the canted mirror. Measurements were made with an infrared camera[1] and with liquid crystals[2]. The infrared camera was also used to observe the heat patterns on the uncooled radial wall of the cavity. For these observations, the cooling was removed near the midplane and throats.

1. I.R. camera and liquid-crystal studies of end-plate temperature patterns

The I.R. camera was sensitive to radiation wavelengths between 1 and 5.5 μm. To avoid difficulties with variations in surface emissivity, the plate was uniformly painted with a flat black paint. The stainless-steel plate would conduct heat relatively rapidly through its thickness before radial diffusion would broaden the temperature patterns.

Temperature studies were also made of the end plates by spraying on pre-blackened liquid-crystal mixtures. Photographs obtained with a camera on colour film indicated the temperature of the various regions on the plate from the colour of the reflected light. Once the final temperature of the transition was obtained, the crystal remained blue in reflected light. Prior to undergoing the transition, the surface is black.

Figure 4 shows typical I.R. camera pictures obtained with the mirror coils at four cant angles. For an uncanted mirror, Fig. 4(a) shows a fairly symmetric annular region. The two small dots visible on the edges are small light bulbs used as heat sources to mark the outer edges of the mirror throat. They are located on the equatorial plane (along a major diameter of the equivalent torus), one "inside" (toward the major axis when the mirror is canted) and one "outside". Figure 4(b) shows an I.R. camera picture taken with a small cant angle of 5°. Now the bright region of the annulus is shifted toward the "inside". It is asymmetrical with respect to the equatorial plane (the plane passing through the two dots). The amount of asymmetry is a function of the cant angle. Figure 4(c) shows a pattern obtained with 7.5° cant angle, about one half the maximum cant angle possible. The annulus has shifted more toward the "inside" and has become more symmetric with respect to the equatorial plane. A bright region of the annulus is visible on the "inside" and indicates the zone where particles with large pitch angle are confined on the "inside" of the minor axis. End losses from this region may be larger because of the increased cold-plasma production from these additional energetic particles, possible space potential effects, and/or the actual end losses of the energetic particles. Figure 4(d) shows an I.R. camera photograph obtained with modest β and a cant angle of 15°. The bright region is reduced on the "inside" now and another bright region appears on the "outside".

Liquid-crystal pictures taken with the magnetic field reversed indicate that the pattern at small cant angles shifts to the other side of the equatorial plane. Figure 5 shows a temperature profile from each of the two field directions at a cant angle of

[1] Bofors I.R. Camera, Mark IRCD-1.
[2] Liquid Crystal Industries, Inc., Turtle Creek, Pa., USA.

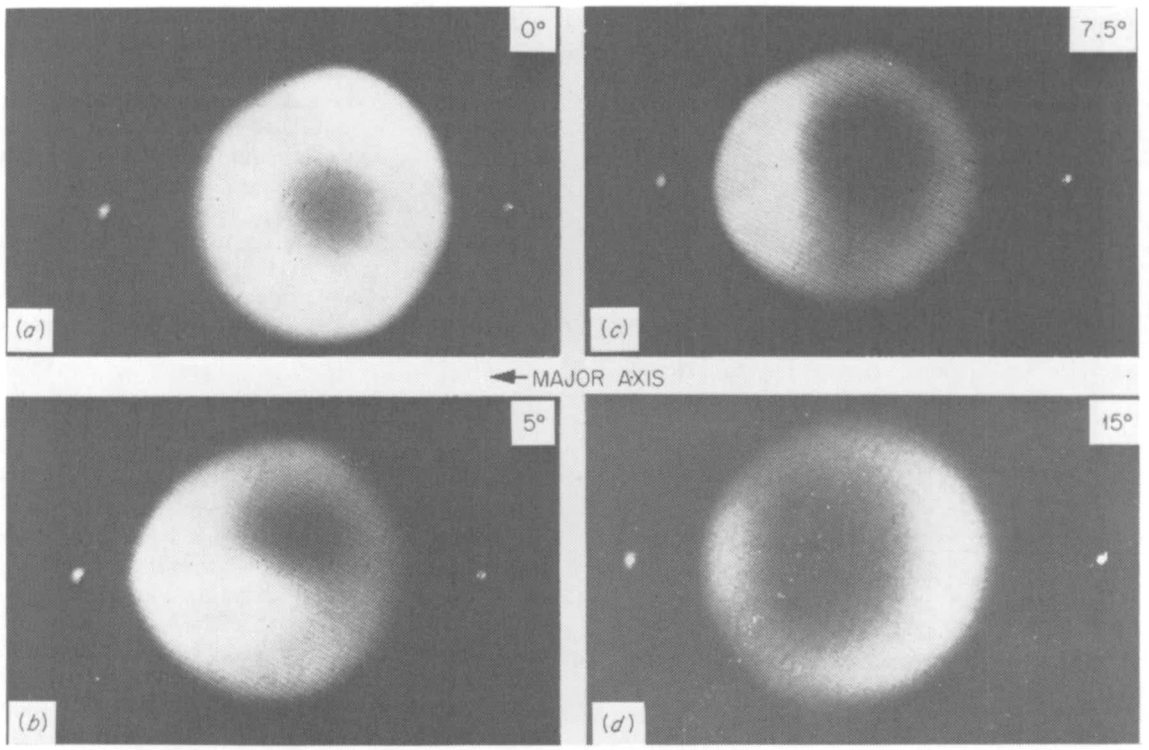

FIG. 4. I. R. camera pictures of end plate: (a) $\theta_c = 0°$; (b) $\theta_c = 5°$; (c) $\theta_c = 7.5°$; (d) $\theta_c = 15°$.

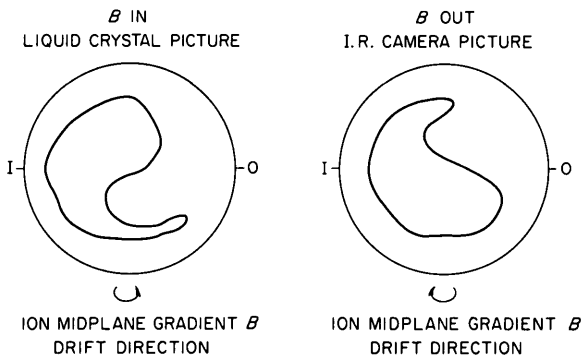

FIG. 5. I. R. camera and liquid crystal temperature profiles with $\theta_c = 4°$ for two magnetic field directions.

4°, one picture taken by I. R. camera and one by liquid crystals. The shift has reversed with the field, indicating that the reflection symmetry is determined by the applied-magnetic-field direction. The asymmetric pattern may be due to an electric field effect on the drift surfaces of the cold plasma, as discussed in section 3. The energetic-electron losses do not show this large asymmetry, indicating that the hypothesized electric field is not large enough to perturb the orbits of the very energetic electrons. As mentioned in section 3, the calculated drift surfaces for energetic particles under the influence of electric fields only qualitatively resemble these figures. However, because of the computing limitations, low-energy particles could not be followed.

Placing large pieces of iron near the machine at several places did not change the pattern for a given cant angle, indicating that the offset is probably not in itself due to an asymmetry in the magnetic field. Again, this observation is in agreement with the calculations of magnetic field errors in section 3.

Measurements were also made with a variety of values of perpendicular stored energy. Some small effects were seen but it was not clear whether these were due to β-effects or merely variations in heating due to the varying amount of cold plasma. Figure 6 shows the variations in the "inner" and "outer" mean position of the pattern (for two cant angles) as a function of the stored energy.

2. Temperature patterns referred to the midplane along field lines

Vacuum field lines were calculated and used to trace back the patterns along field lines from the end plates to the midplane. The maximum temperature points from both the I. R. camera measurements and the liquid-crystal measurements were traced back along these field lines to the midplane. Figure 7 shows the maxima as a function of cant angle for points on the "inside"

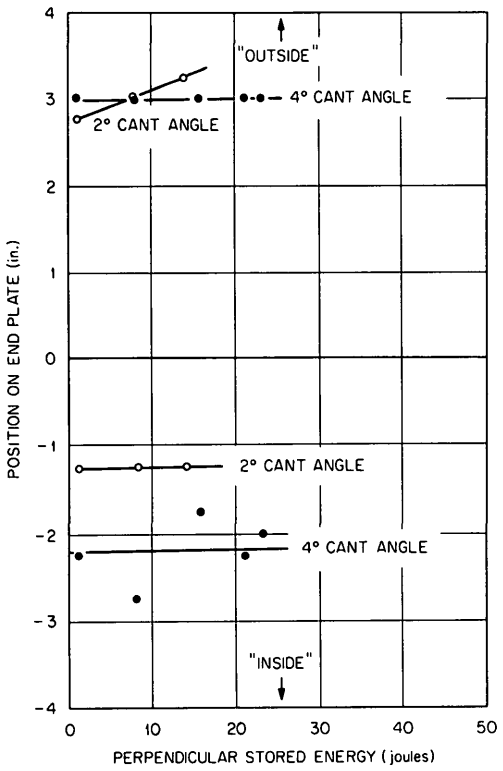

FIG. 6. "Inner" and "outer" mean positions of the annulus as a function of stored energy. Cant angle is the parameter.

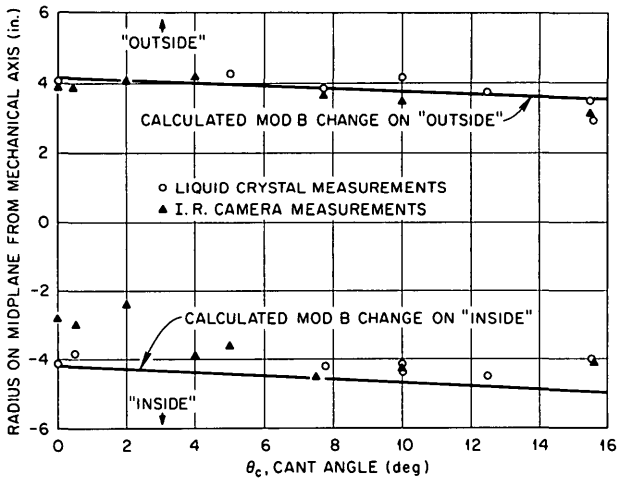

FIG. 7. "Inside" and "outside" maxima of temperature profiles as a function of cant angle from liquid crystal and I.R. camera measurements. The modulus-B motion with cant angle is also shown.

and "outside" on the equatorial plane. Both I.R. camera and liquid-crystal pictures give about the same displacement, showing that the source of energy producing these patterns moves toward the major axis as the mirror is canted.

Also shown in the figure is the zero-β, modulus-B motion as a function of cant angle for that value of B which corresponds to the maximum temperature point of the liquid-crystal temperature patterns for the uncanted mirror condition. The positions for the modulus-B motion were also deduced from the magnetic-field calculations.

The temperature patterns appear to follow the motion of the modulus-B contour both "inside" and "outside". The agreement between the calculations and experiment remains good up to the maximum cant angle of $\sim 15°$.

We conclude that the region near the midplane which produces the maximum temperature on an end plate moves on a modulus-B surface for modest-β plasmas. High-β (or large stored energy) effects are not large.

3. I.R. camera studies of the radial wall of the canted mirror

Figure 8 shows the temperature patterns measured by the I.R. camera looking at the radial wall of the canted mirror experiment. The camera is off the midplane at an angle $\sim 20°$ looking at the cavity and one field coil. The cavity was stripped of all the normal cooling. The large round dark areas are cool ports. The slanted dark lines are cool diamagnetic flux loops. The two photographs of the figure show the difference between canted and uncanted operation. Note the appearance of a "hot spot" that develops in the lower portion of the figure which is toward the "inside" of the torus along a major diameter. This is the point towards which the drift surfaces move when the coils are canted. The "hot spot" is always present when canted whether or not a high-β plasma is present (i.e. whether or not off-resonant power is used or whether or not skimmer probes are used to remove the high-β annulus). However, the spot is "hotter" with off-resonant power and with the probes out, indicating that some energetic plasma from the annulus strikes this region during the canted operation. Temperature and time measurements show that only a very small fraction of the total power is dissipated here (< 1%), hence this heating does not represent a serious loss of energy.

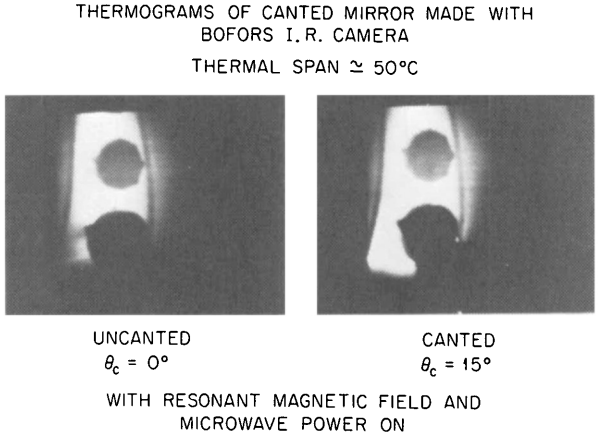

FIG. 8. Temperature patterns on midplane of canted-mirror experiment under canted and uncanted operation showing "hot spot" on "inside" with canting.

D. END-PLATE X-RAY SCANS

A scanning X-ray detector was mounted on the stainless-steel end plate. This device scanned along a diameter in the equatorial plane of the equivalent torus and detected "soft" X-rays. The detector was an air ionization chamber similar to those mounted in probes and described in a previous publication [9]. It was collimated within a lead block and had a spatial resolution, δr, of $\sim \frac{1}{2}$ in. The "soft" detector was sensitive to X-rays below $\sim$ 100 keV.

The X-ray detector gave results consistent with the photographs of a scintillating end plate, described in section 4.B. With an uncanted mirror, Fig. 9 shows the signal as a function of position from the minor magnetic axis to the "inside" edge of the end plate.

Since the X-ray intensity and power deposition are approximately circularly symmetric about the magnetic axis, and since the intensity or power deposition at large radii are lower because they are spread over a larger area, a correction can be applied. We multiply them by a factor proportional to the area of the annulus at the detector centre, $2\pi r\delta r$, divided by the area covered by the detector resolution, $\pi(\delta r/2)^2$. The resulting quantity for both X-rays and temperature patterns are plotted in Fig. 10 as a function of the midplane crossing radius of the field line that passed through the detector. We also plot the curve of $\Delta\phi(r)/\Delta r$, the radial derivative of the diamagnetic signal versus skimmer probe radius on this plot.

Note that all signals peak at about the same radius ($\sim$4.5 in.), indicating that they all give approximately the same indication of the mean radius of the maximum in the annulus.

As the mirror is canted, the pattern shifts "inward" toward the major axis and develops a double peak at small cant angles which merge into one peak at larger cant angles ($\theta_c \gtrsim 6°$). The peak remains in essentially the same place on the end plate for larger cant angles.

For cant angles less than 6°, the peak position is a function of the amount of stored energy. Figure 11 shows the position of this peak as a function of cant angle for two values of stored energy. Clearly, the peak shifts towards the "outside" away from the wall for the larger values of β as long as the cant angle is less than 6°. For larger cant angles, there is no perceptible change with stored energy. The change with high-β observed for small cant angles is in the favourable direction to decrease the losses to the walls.

E. DIAMAGNETIC DETERMINATION OF THE HIGH-β ANNULUS POSITION AND LENGTH

This diagnostic technique consisted of measuring the plasma diamagnetic field at 23 positions. The field is measured by electronically integrating in time the flux change through 23 small (< 1-in.diam.) multiturn coils as the plasma decays after the

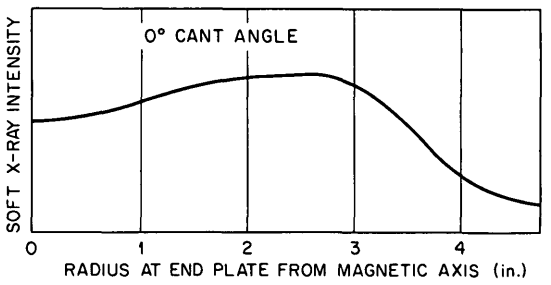

FIG. 9. Soft X-ray signal versus radius on end plate for $\theta_c = 0°$.

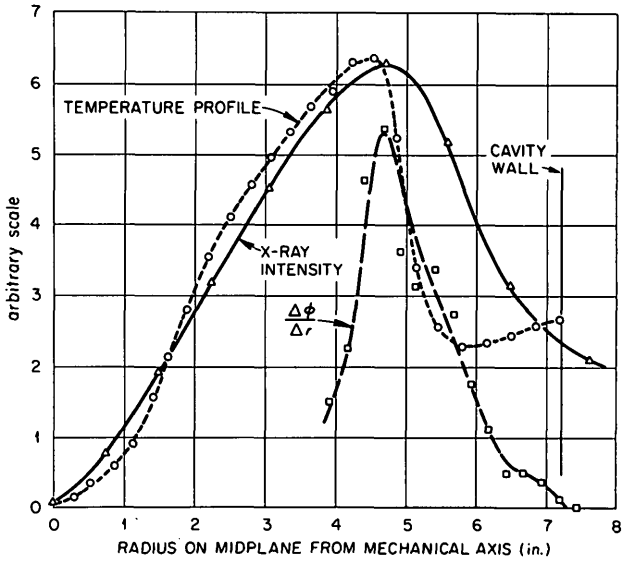

FIG. 10. End-plate X-ray intensity, end plate temperature, and $\Delta\phi/\Delta r$ all referred to midplane for $\theta_c = 0°$.

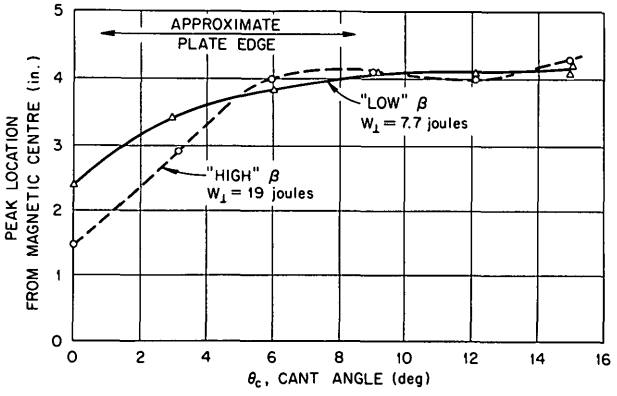

FIG. 11. End-plate X-ray peak versus cant angle for two values of stored energy.

microwave power is turned off. The coils are placed at $1\frac{1}{2}$-in. intervals along the cavity axis, along a line 8 7/8 in. from the axis toward the outside of the torus and along a radius in the midplane outside the cavity. All coils measure the change in the axial component of the diamagnetic field (ΔB_z). A similar technique has been used on the ELMO facility [1].

The data were analysed by two techniques. The first was a simple multiple loop approximation to the plasma currents; the second was a sophisticated equilibrium calculation. We describe the first technique here because it is simple and straightforward. Probably because of its simplicity, however, the calculation did not produce a model in agreement with the other diagnostics.

The plasma was represented by two axisymmetric arrays of current loops, evenly spaced along the axis with the current in each set of loops divided equally among its loops. The plasma was characterized by five parameters: half length, L; radii, A_1 and A_2; and currents, I_1 and I_2. Figure 12 shows the configuration. The number of loops could be varied but it was generally found that a total of 8 loops gives as good a fit as is meaningful. Such a current distribution represents approximately an annular plasma with constant pressure over a rectangular minor cross-section.

A computer program was used which sequentially varied the three parameters A_1, A_2, and L in order to minimize the quantity

$$U_M = \sum_{i=1}^{23} (\Delta B_{meas} - \Delta B_{calc})^2$$

and the currents I_1 and I_2 are calculated for each set of parameters in order to satisfy exactly the equations

$$\Delta B_{calc}(0, 0) = \Delta B_{meas}(0, 0)$$

and

$$\int_0^\infty \Delta B_{meas}(0, Z)dZ = \mu_0 (I_1 + I_2)$$

The method provided a measurement of the half-length and mean radius, but it was impossible with measurements accurate to a few per cent to find the thickness of the plasma with coils not in contact with the plasma.

The half-length and mean radius were measured as a function of stored energy, resonance zone position, and cant angle with the other parameters held fixed. The mean radius was remarkably constant at $\sim 3\frac{1}{2}$ in. for all conditions as if the plasma were tied to some physical feature of the cavity or vacuum magnetic field. This radius was smaller than the radius measured with skimmer probes or end plate diagnostics. The plasma shortened as the stored energy or cant angle

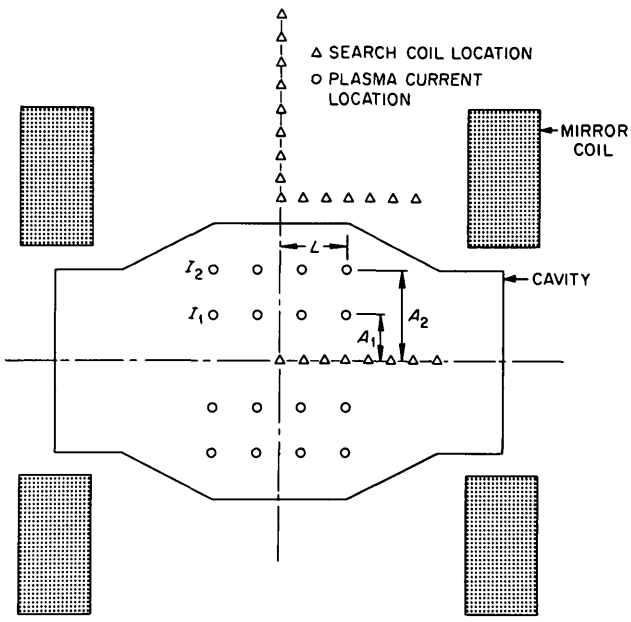

FIG. 12. Location of search coils and equivalent plasma current loops.

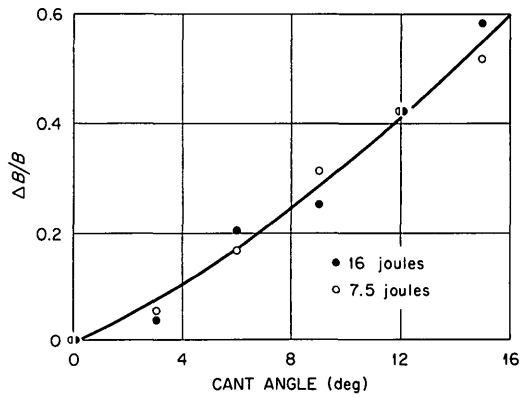

FIG. 13. ΔB/B versus cant angle for two values of stored energy, indicating a displacement of the plasma toward the "inside" with increasing cant angle.

was increased. There was no systematic change in length as the cold-electron-cyclotron resonance zone was moved.

The second technique was a very sophisticated analysis of the diamagnetic probe data by Hedrick [10]. It gave a mean radius and width more in agreement with the end plate and skimmer probe measurements. This latter calculation, however, was used only on the data for the uncanted mirror. Because of its complexity, it was not used to examine the canted data.

From the measurements mentioned earlier, it is known that the plasma moves toward the toroidal major axis (the inside) when the coils are canted. In the low-β limit, the magnitude of this displacement can be easily calculated. It is of

interest to know whether this displacement is modified by the finite β, and, in particular, whether the β tends to recentre the plasma on the minor axis. The shift was measured by subtracting the signals from a pair of coils located on the inside and outside of the torus in the mid-plane just outside the cavity wall. The difference signal, ΔB, when normalized by dividing by the signal from one coil, should be a monotonic (linear for $\Delta B/B \ll 1$) function of the radial displacement of the plasma. This signal is plotted versus cant angle in Fig. 13 for two values of stored energy. There is no significant difference between the two sets of data, implying that for the values of β for which these data were taken the inward displacement of the plasma is not β-dependent. The 16-joule curve gives a β of ~ 0.57 if we assume the annulus is 1-in. thick. Here, as in other experiments, it was not possible to take reproducible data at the maximum β-values obtainable.

5. CONCLUSIONS

The canted-mirror experiments have shown that the relativistic high-β annuli first observed in ELMO are preserved in an asymmetric system and are available for the stabilization of a toroidal plasma. Under the canting operation, the annulus moves as predicted toward the major axis of the torus. Particles escaping out of the mirrors are found to be in the region expected on the basis of single-particle drift calculations. High-β effects displace the energetic lost particles toward the outside. The use of non-conducting glass end plates has suggested that the relativistic annuli might be stable in a torus without line-tying. Hence, these annuli may be used to provide the proper field gradients to stabilize a toroidal plasma. Effects attributable to an electric field are observed to cause an asymmetry in the mirror losses of cold plasma.

ACKNOWLEDGEMENTS

We are indebted to many members of the Thermonuclear Division for numerous helpful discussions. C. L. Hedrick and C. E. Parker were invaluable in making the calculations of vacuum magnetic fields. G. E. Guest provided valuable criticism of and contributions to the theoretical section. The conscientious technical assistance of R. L. Livesey and M. W. McGuffin was of great value. We are indebted to K. V. Cook of the Metals and Ceramics Division of Oak Ridge National Laboratory for the use of the I. R. camera. The continued support and encouragement of H. Postma is gratefully acknowledged.

REFERENCES

[1] DANDL, R.A., EASON, H.O., EDMONDS, P.H., ENGLAND, A.C., in Relativistic Plasmas (Proc. The Coral Gables Conf., BUNEMAN, O., PARDO, W.B., Eds), Benjamin, New York (1968) 181; also, DANDL, R.A., EASON, H.O., EDMONDS, P.H., ENGLAND, A.C., in 2ème Colloque Intern. sur les Interactions entre les Champs Oscillants et les Plasmas (CONSOLI, T., Ed.), (Proc. Coll. Saclay, 1968) 1, University of France Press, Paris (1968) 161.

[2] GIBSON, G., JORDAN, W.C., LAUER, E.J., Phys. Fluids 6 (1963) 133.

[3] GUEST, G., HEDRICK, C.L., HOGAN, J.T., Phys. Fluids 15 (1972) 1159.

[4] KADOMTSEV, B.B., in Plasma Physics and the Problems of Controlled Thermonuclear Reactions, Pergamon Press, New York, 3 (1959) 340, and 4 (1959) 417.

[5] MOROZOV, A.I., SOLOVEV, L.S., Sov. Phys.-Tech. Phys. 30 (1960) 241; MOROZOV, A.I., SOLOVEV, L.S., in Reviews of Plasma Physics (LEONTOVICH, M.A., Ed.) 2 (1966) 267 ff.

[6] GIBSON, G., JORDAN, W.C., LAUER, E.J., WOODS, C.H., Phys. Fluids 7 (1964) 548.

[7] SPROTT, J.C., Phys. Fluids 16 (1973) 1157.

[8] GUEST, G.E., HARRIS, E.G., Phys. Rev. Lett. 27 (1971) 1500.

[9] DANDL, R.A., EASON, H.O., EDMONDS, P.H., ENGLAND, A.C., GUEST, G.E., HEDRICK, C.L., HOGAN, J.T., SPROTT, J.C., in Plasma Physics and Controlled Nuclear Fusion Research (Proc. 4th Int. Conf. Madison, Wisconsin, 1971) 2, IAEA, Vienna (1971) 607.

[10] HEDRICK, C.L., private communication.

(Manuscript received 21 May 1973)